Acta Mechanica Slovaca **28 (2): 28 - 43,** Jun **2024**
https://doi.org/10.21496/ams.2024.007

Acta Mechanica SlovacaISSN 1335-2393
www.actamechanica.sk

Modelling of Pulsed Flow Effects Through the Exhaust System of a Turbocharged Engine Using Mixed Flow Turbine

Djamel Mazari [1], Mustapha Bordjane [2*], Mohammed Hamel [2], Khadidja Boualem [3]

[1] University of Ibn Khaldoun-Tiaret(14000), Algeria
[2] University of Sciences and Technology Mohamed Boudiaf-Oran(31000), Algeria
[3] University of Relizane-Relizane(4800), Algeria

Abstract: For some decades, reductions of fuel consumption and pollutant emission control have become the first requirement for internal combustion engines. Turbocharging is a promising way among many techniques to solve this problem since it leads to a downsized, lighter and more compact engine. Two important novelties can be listed in this study, the first is the development of a thermodynamic (zero dimensional) model for the gas expansion process through the exhaust system of turbocharged internal combustion engines. The latter is used to setup the unsteady state analysis using interpolation function for cyclic time of the internal combustion engine and the boundary conditions at the exhaust manifold inlet. The second point is the study of the complete exhaust line from the valves ports to the turbine diffuser including the exhaust manifolds which has strong influences on the flow characteristics at the volute inlet. Numerical investigation using three dimensional, viscous, turbulent and compressible flow is performed. In the first step, a steady state simulation is considered just to validate the computational results. In the second step, an unsteady state is planned with conditions like those encountered in real applications. Numerical results from mixed-flow turbine used as test case, are presented. The results include performances and flow characteristics, predictions of blade loading, cyclic pressure, cyclic mass flow rate, inlet-outlet flow parameters and flow structure.

Keywords: Turbocharging; modelling; blade loading; flow structure; unsteady state analysis.

1. Introduction

Generally, turbomachine sizing reflects initial conditions in which it must be operated at optimal efficiency but, during their exploitation, usual off-design operating points occur and where the situation changes. So, two methods are used to predict the machine reaction at this situation. Formerly, empirical and theoretical methods were tedious and longer. Recently, with developed methods and availability of software and hardware computers, numerical investigations can be eventually conducted in this situation, where geometry is complex and the flow is transient, turbulent and compressible. CFD methods and analysis consider the 3D, viscous and unsteady characters of flow. Hence, they provide accurate information to designers about the fluid behavior inside the machine. Throughout the last decades, the common evolution of computer tools and numerical methods play a part to the great advances in the sizing and analysis of turbomachinery.

Principally, the output power of an engine depends on the amount of fuel that can be burned in the combustion chamber. The latter quantity is defined by the critical

*** Corresponding author:** Mustapha Bordjane, ***E-mail address:*** *mustapha.bordjane@univ-usto.dz;*

factor of the mass of air that can be admitted. Increasing its density by boosting the load must be a solution to increase the output power per unit of weight and size of the engine [1]. The large amount of heat released from combustion process is wasted in internal combustion engines within exhaust gas after it is used partially to move the piston during the expansion stroke and within the three heat transfer modes. Around 40% of the fuel energy is wasted in the form of heat through the exhaust while another 30% is lost in the engine coolant [2]. Generally, engine exhaust gas energy consists of thermal energy, pressure energy and kinetic energy. Recovery methods of exhaust gas energy aim at recovering the exhaust gas pressure energy. Additional expansion devices, such as power turbines, have potential to expand further exhaust gas inside the energy recovery [3].

Based on the turbocharged system principles, if the contents of cylinder at exhaust valve opening (EVO) are somehow allowed to be expanded in an isentropic way and reversibly down to the ambient pressure, the work that could be done is potentially available to drive a turbocharger turbine placed in the exhaust manifold outlet. The most of turbocharged engines use the principle of pulse pressure instead of constant pressure since the full advantage has been taken of the pulse energy, which is the kinetic energy of exhaust gas leaving the exhaust valves. So, the high gas velocity leaving the port is converted to a pressure rise in the manifold. Hence, the objective is to make the maximum use of the high pressure and temperature which exist in the cylinder when the exhaust valve opens, even at the expense of creating highly unsteady flow through the turbine [4]. This requires the exhaust manifold inlet pressure to suddenly rise to the end of expansion stroke pressure when the exhaust valve first starts to open, then falls progressively through turbine to the ambient pressure [5]. However, for temperature and since the expansion of the gases inside the cylinder during the exhaust process is very nearly isentropic, exhaust temperature in practice could be regarded as fixed for a given exhaust process.

The choice of the turbine depends on the application though it is not always clear that any one type is superior. For automotive applications, turbochargers with radial turbines are much lighter, simpler, more compact and less costly. However, the optimum efficiency of the latter is limited to a higher blade speed ratio whereas; the peak efficiency of the mixed flow turbine is at lower value of this parameter [5]. With mixed-flow turbine, it is also possible to perform more satisfactory efficiency characteristics, which has an important influence on the performance of the turbocharger engine.

Taking into account the pulsating effect of flow has preoccupied researchers for several decades. It is, however, still the subject of several studies in different fields, analytical, numerical and even experimental. In this study, a thermodynamic model is developed for the gas expansion process through the exhaust system of turbocharged internal combustion engines. Then, the model is used to setup the unsteady state analysis using interpolation function for cyclic time of the internal combustion engine.

For the application side of the model developed, mixed-flow turbines are used. Physical model considered in this work is the complete exhaust line from valves ports to the turbine diffuser including the exhaust manifolds which has strong influences on the flow characteristics at the volute inlet. The most previous studies treat the steady state flow through these types of turbines just from the volute inlet to the diffuser outlet by means of imposed inlet conditions. Checking of blade loading which have an important role for the sizing and design of the turbine rotor, was established. Finally, flow structure which leads to obtain a 3D flow description is presented and which in turn helps to make an initial estimation on the flow regularity.

2. Thermodynamic model

Based on the diagram cycle (p-V, Figure 1) established from a detailed thermodynamic study using the engine data given by the designer, during the expansion stroke and for a single cylinder, the gas volume varies from combustion chamber volume (V_{cc}) to (εV_{cc}), where e is the compression ratio. On the other hand, during the combustion process, gas volume varies from (V_{cc}) to (ρV_{cc}), where r is the volume increase ratio during combustion.

According to the Thermodynamic (0D) Model, it is assumed that the expansion process is continued in an isentropic mode through the exhaust manifold and the turbine stage (section b-0 of the diagram). As consequence, the thermodynamic relations used for the gas polytropic transformation to stand out the pressure and temperature signals imposed at

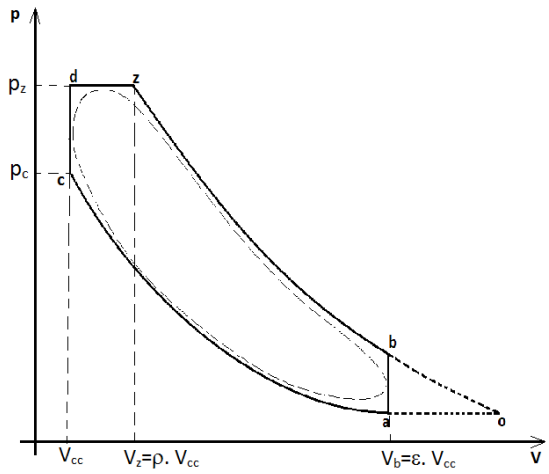

Figure1: p-V diagram for ideal Diesel cycle

the exhaust manifold inlets are the following:

$$TV^{n-1} = C^{st} \quad (1)$$

$$TV^{n-1} = C^{st} \quad (2)$$

So, if we refer (p_b, V_b) to the pressure and volume at the end of expansion stroke, and (p_z, V_z) to the pressure and volume at the end of combustion process which is the beginning of the expansion stroke, pressure at the end of expansion stroke can be obtained:

From (1):

$$p_b = p_z \cdot \left(\frac{V_z}{V_b}\right)^{n_2} = p_z \cdot \left(\frac{\rho V_{cc}}{\varepsilon V_{cc}}\right)^{n_2} = p_z \cdot \left(\frac{\rho}{\varepsilon}\right)^{n_2} \quad (3)$$

Here, n_2 is the polytropic exponent (n_2=1.23). At the beginning of the expansion stroke, $V_z=\rho V_{cc}$ and at the end of the expansion stroke, $V_b=V_{totcyl}=\varepsilon V_{cc}$.

The volume increase ratio during combustion process can be calculated from: $\rho=(\beta_z/\lambda).(T_z/T_c)$ where β_z is the coefficient of volume variation during the combustion process, which can be calculated from the empirical correlation (from our thermodynamic study, β_z=1.0297). l is the pressure increase ratio during the combustion process given by: $\lambda=(p_z/p_c)$ where pz is the pressure at the end of combustion process and pc is the pressure at the end of compression stroke. In the same manner for the temperature:

From (2):

$$T_b = T_z \cdot \left(\frac{V_z}{V_b}\right)^{n_2-1} = T_z \cdot \left(\frac{\rho}{\varepsilon}\right)^{n_2-1} \quad (4)$$

Now, the expansion prosecution of gases (section b-0 of the diagram) in the exhaust manifold and the turbine stage is supposed which implies the increase of compression ratio (ε) from 18 (inside the cylinder) to that corresponding to the turbine stage exit conditions. Pressure and temperature evolutions versus compression ratio (ε) based on relationship (3) and (4) are represented (Fig.2). From our thermodynamic study: p_z=14.6654MPa, p_c=11.9230MPa, T_z=1920K, T_c=1092K. As a result, λ=1.23 and ρ=1.4727, with the pressure and temperature can be calculated or estimated at the end of the expansion stroke (manifold inlet) and at the turbine stage exit from expressions (3) and (4).

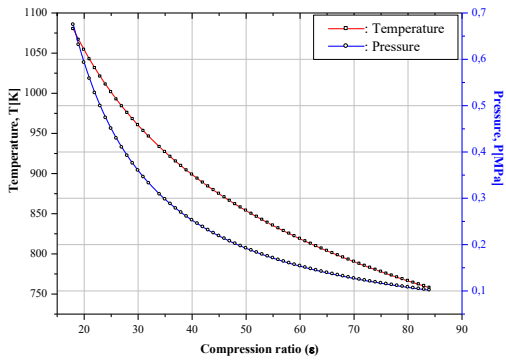

Figure 2: Gas expansion prosecution for turbocharged cycle

3. Mathematical formulation

Analysis methods of systems are based on the mathematical descriptions of various facts, events and processes. Mathematical model construction is the key to system analysis. Simulation model has a phenomenology basis, the model must accurately reproduce the phenomenon studied. Multi-dimensional models provide qualitative and quantitative information about the flow field at particular times and locations within the combustion chamber [6]. The equations used to evaluate the unsteady state gas flow in manifolds of internal combustion engines are derived in several forms. The most complete mathematical description of fluid flows are the Navier-Stokes equations

(including continuity and energy) in 3D, supplemented by empirical laws relating the dependence of viscosity and thermal conductivity to the flow variables and by thermodynamic state relationships [7]. Time-averaging operation on the Navier-Stokes momentum equations result in the Reynolds-averaged Navier-Stokes equations.

3.1 Continuity equation

$$\frac{\partial \rho}{\partial t}+\frac{\partial}{\partial x_j}\left(\rho U_j\right)=0;\left(j=1,2,3\right) \tag{5}$$

3.2 Reynolds averaged momentum equations

$$\frac{\partial\left(\rho Ui\right)}{\partial t}+\frac{\partial}{\partial x_j}\left(\rho U_i U_j\right)=-\frac{\partial p}{\partial x_i}+\frac{\partial}{\partial x_j}\left[\tau_{ij}-\rho\overline{u_i u_j}\right] \qquad \tau_{ij}=\mu\left(\frac{\partial U_i}{\partial x_j}+\frac{\partial U_j}{\partial x_i}\right);-\rho\overline{u_i u_j}=\mu_t\left(\frac{\partial U_i}{\partial x_j}+\frac{\partial U_j}{\partial x_i}\right)-\frac{2}{3}pk\delta_{ij} \tag{6}$$

3.3 Energy equation

$$\frac{\partial\left(ph_{tot}\right)}{\partial t}-\frac{\partial p}{\partial t}+\frac{\partial}{\partial x_j}\left(\rho U_j h_{tot}\right)=\frac{\partial}{\partial x_j}\left(\lambda\frac{\partial T}{\partial x_j}+\frac{\mu_t}{\mathrm{Pr}_t}\frac{\partial h}{\partial x_j}\right)+\frac{\partial}{\partial x_j}\left[U_j\left(\tau_{ij}-\rho\overline{u_i u_j}\right)\right] \tag{7}$$

3.4 SST turbulence model

The shear-stress transport (SST) k-ω model has been developed by F.R. Menter [8] to effectively blend the robust and accurate formulation of the k-ω model in the near-wall region with the free-stream independence of the k-e model in the far field. It is more accurate and reliable for a wider class of flows (e.g., adverse pressure gradient flows). The two transport equations of SST model are given by:

$$\frac{\partial K}{\partial t}+\frac{\partial}{\partial x_j}\left(\overline{U}_j K\right)=\left[\left(\nu+\frac{\nu_t}{\sigma_k}\right)\frac{\partial K}{\partial x_j}\right]+P_K-\beta^* K\overline{\omega} \tag{8}$$

$$\frac{\partial\overline{\omega}}{\partial t}+\frac{\partial}{\partial x_j}\left(\overline{U}_j\overline{\omega}\right)=\frac{\partial}{\partial x_j}\left[\left(\nu+\frac{\nu_t}{\sigma_{\varpi_1}}\right)\frac{\partial\overline{\omega}}{\partial x_j}\right]+P_{\overline{\omega}}-\beta\overline{\omega}^2+2\left(1-F_1\right)\sigma_{\overline{\omega}2}\frac{1}{\overline{\omega}}\frac{\partial K}{\partial x_i}\frac{\partial\overline{\omega}}{\partial x_i} \tag{9}$$

$$F_1=\tanh\left(\xi^4\right);\xi=\min\left[\max\left\{\frac{\sqrt{K}}{\beta^*\overline{\omega}y},\frac{500\nu}{y^2\overline{\omega}}\right\},\frac{4\sigma\varpi_2 K}{CD\varpi y^2}\right];\nu_t=\frac{\alpha_1 K}{\max\left(\alpha_1\overline{\omega},SF_2\right)};$$

$$\overline{\omega}=^{\varepsilon}/K.\beta^*.;.P_{\overline{\omega}}=\alpha\frac{P_k}{\nu_t}.;.F_2=\tanh\left(\eta^2\right);..\eta=\max\left\{\frac{2\sqrt{K}}{\beta^*\overline{\omega}y},\frac{500\nu}{y^2\overline{\omega}}\right\}$$

Where:

y: is the nearest distance from walls and n is the kinematic viscosity

F1 and F2: are the corrective functions, its formulation is based on the nearest distance to walls and flow variables. S value is a function of the strain rate. Table1, below summarizes the model constants.

Table1: SST model constants

Symbols	β*	β	σ_k	$\sigma_{\omega 1}$	a	$\sigma_{\omega 1}$	a_1
values	0.09	0.0828	2.0	2.0	2.0	1.1680	0.31

4. Numerical procedure

The MFT rotor (Figure 3), is tested under steady and transient states. To integrate the PDE system, the finite volume method was used. For discretization schemes, which is well known that many problems in fluid mechanic applications are dominated by discontinuities as shock waves and contact surfaces or high gradients of the flow variables. So, the idea is to combine the use of high-resolution scheme for advection terms and the first order backward Euler scheme for transient terms or temporal derivatives. As demonstrated previously, the advantage of first order scheme is that a monotone variation is achieved for the numerical flow-field properties in the vicinity of discontinuities. To account for transient interaction effects at the sliding interfaces or frame change, transient rotor-stator model (TRS) and the general grid interface (ggi) method are used. SST model was used to handle turbulence quantities. SEMPLEC algorithm was used to treat the pressure-density correlation in the case of compressible flow. The considered configuration is that relative to the assembly: exhaust manifold, volute, rotor and diffuser, components of the complete exhaust line of turbocharged engine (Figure 3).

Data of the six cylinders, four strokes cycle engine (MIDR 0635 40 M/3) and the geometric information of the mixed flow turbine are summarized in table. 02 and table. 03 below.

Table 2: Engine characteristics

Engine characteristics	Values
Displacement[l]	12.02
Stroke [mm]	140
Diameter [mm]	135
Compression ratio	18/1
Firing order	1-5-3-6-2-4
Mean piston speed [m/s]	9.33
Maximal power [kW]	235
Maximal Torque [N.m]	1450

Table 3: MFT geometric information's [12]

Turbine characteristics	Values
Blade number	12
Hub exit radius	13.5
Inlet blade angle (β_b)	20°
Rotor length, L [mm]	40
Rotor inlet mean diameter, d2,m [mm]	84
Rotor inlet blade height, b_2 [mm]	18
Tip radius (hub), r_{H2} [mm]	36
Tip radius (shroud), r_{S2} [mm]	47.5
Exit radius (shroud), r_{S3} [mm]	39

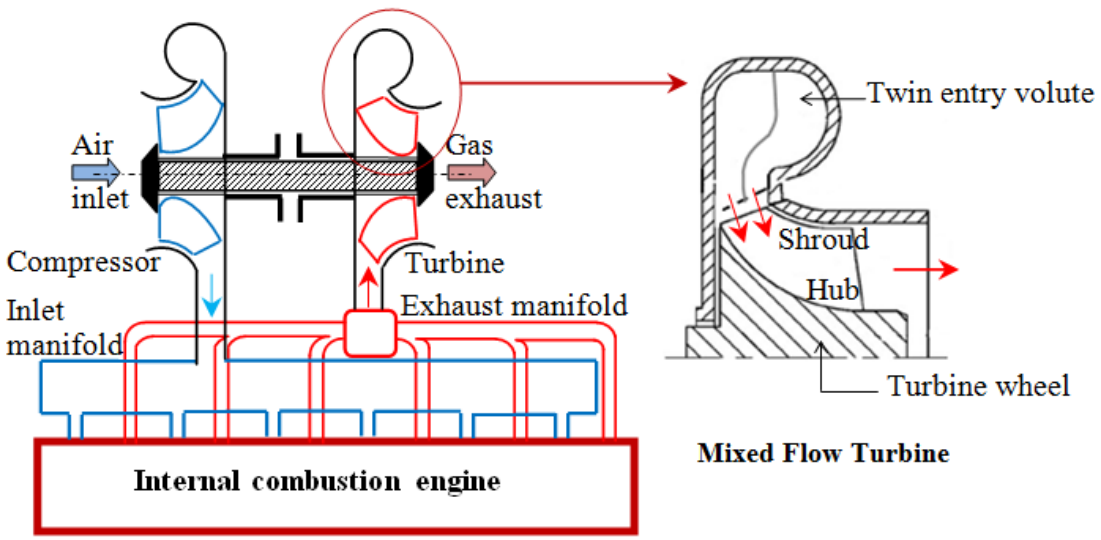

Figure 3: Configuration of the system considered and geometric detail of turbine rotors

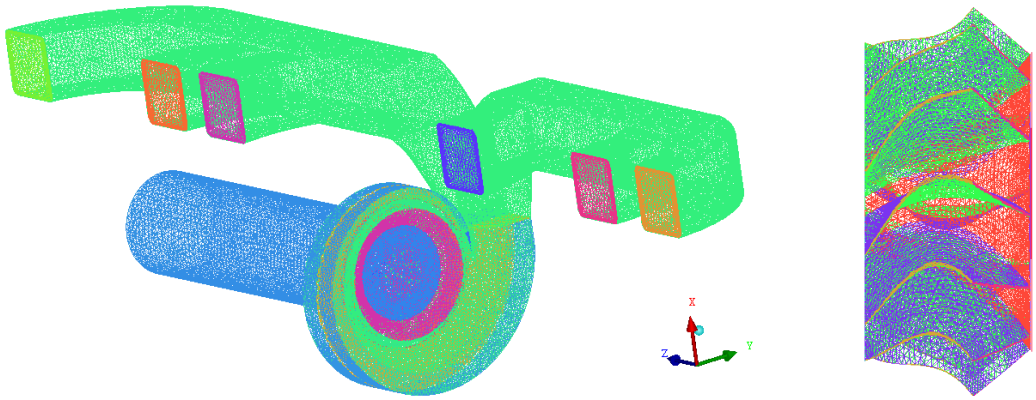

Figure 4: Mesh configuration

4.1 Geometry and mesh generation

The tetrahedral grid is automatically generated in the interior of the volume using the surface grid as starting point. The finest meshes produced results that can be considered mesh independent for the unstructured models. The final fine unstructured mesh used in this study, in compromise with CPU time, contains (2535454) tetrahedral cells for the assembly (exhaust manifold, volute and rotor with diffuser) (Figure 4).

Grid sensitivity study was also carried out (Fig. 5). Grid size is always a limiting factor in any CFD study. Therefore, performing grid sensitivity studies to guarantee mesh independent results was required.

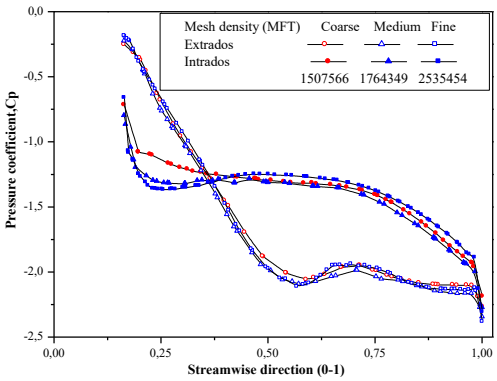

Figure 5: Grid sensitivity of pressure coefficient for MFT

4.2 Steady state simulation

For steady state simulation, mass flow rate and temperature of exhaust gases are imposed at exhaust manifold inlets. At the outlet of the diffuser, the static pressure is specified. At steady-state operating, the performance of each cylinder is essentially the same, due the steady-state functioning of the governor clutch resulting in the same amount of the injected fuel per cycle [9].

Figure 6 shows inlet and outlet boundary conditions. The inlet temperature from thermodynamic calculations was taken as 900K and the measured total mass flow rate given by the constructor was 0.47kg/s. It should be mentioned that the mass flow rate equally divided into the six inlets of the exhaust manifold and assumed that all the inlets received one sixth of the total mass flow rate simultaneously (0.078 kg/s). Rotational speed of the rotor based on operating data of the turbine was 98000rev/min. Since isentropic exhaust gas process was supposed, adiabatic walls during this stroke, are specified. At the end of expansion process through the turbine stage, flow velocity tends to reduce to zero. Hence, dynamic pressure vanished and therefore, the specified pressure is the static one. So, at the outlet of exhaust tube, P_{spe}=0.101325MPa. The wall-function approach of Launder and Spalding [10] is used to provide near-wall boundary conditions for the mean flow and turbulence transport equations.

4.3 Transient state simulation

At transient operating, each cylinder experiences different fueling during the same engine cycle due to the continuous movement of the fuel pump rack initiated by the load or speed change and hence, significantly affects the whole engine operation [9]. For the transient state simulation, six engine regimes are considered (1600, 1700, 1800, 1900, 2000, and 2200) rev/min corresponding to the time cycle of simulation (0.075, 0.0706, 0.0667, 0.06316, 0.060, and 0.0545) s. Pulse frequency or the frequency associated

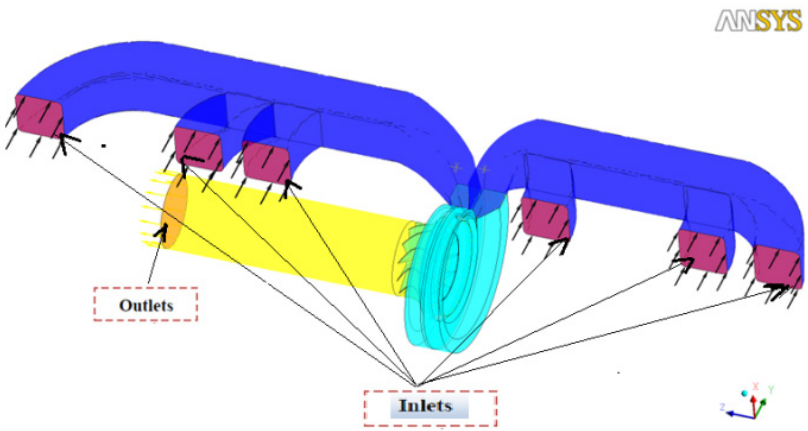

Figure 6: Planes for boundaries conditions specification

to natural period of explosion, function of cylinders number (n_c) and engine regimes (N) are given by: f=(n_c/2). N/60 Hz, the corresponding frequencies are given by (80, 85, 90, 95, 100 and 110) Hz. The speed of the turbines directly depends on the engine. It is driven instantaneously by the engine exhaust gases. Hence, from turbocharging speed versus engine speed curves available in specialized literature, the corresponding rotor speeds of the turbine are (96000, 98000, 103000, 106000, 110000 and 120000) rev/min. To ensure convergence and to respect the CFL number, the time steps corresponding for each cycle are respectively (125, 117.67, 111.11, 105.2, 100 and 90.83).10-6 s. So, the pressure signal imposed in the inlet of exhaust manifold just at the opening of exhaust valves based on the firing order (1-5-3-6-2-4) and consequently the exhaust phases succession (2-4-1-5-3-6), is given by (Figure 7).

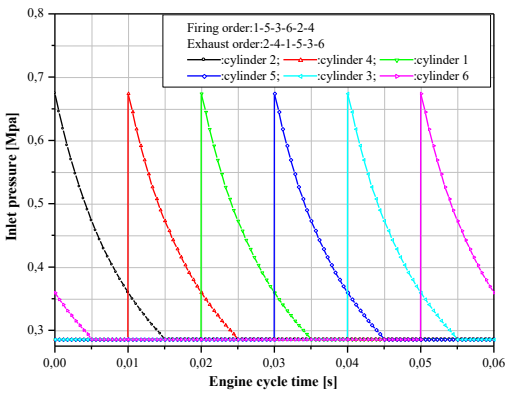

Figure 7: Inlet pressure signal for unsteady state solution

5. Results and discussion

5.1 Results from steady state solution

Results presented for the steady state are just to validate our numerical model. Generally, for the configuration considered, measuring pressure distribution along the shroud profile is used to check numerical predictions. Also, it is an indicator parameter of losses occurring inside rotor channel.

Figure 8, (a) and (b) show the static pressure against the axial distance of MFT rotor. Computed static pressure of the mixed-flow turbine for two pressure ratios are compared to the measured static pressure [11, 12]. The latter authors treat experimentally the same mixed-flow rotor geometry at the same steady state conditions. In Figure 8 (a), for the pressure ratio of (PR=2.81) and in Figure 8 (b), for the pressure ratio of (PR=2.90). From these figures, we observe nearly the complete conversion of pressure energy of the exhaust gases to drive the rotor. Expansion of gases through the rotor is also regular. From this observation, the shroud distance or size to have the complete conversion of energy can be obtained. In MFT rotor, the exhaust gas expands rapidly at the beginning from the leading edge as indicated by the sharp drop in the shroud pressure. After that, it expands linearly within slightly higher slope until the blades trailing edge (BTE). From the trailing edge, the pressure holds nearly constant.

The predicted, shroud and hub pressures at blade leading edge (BLE), are shown in Figure 9, compared to the measured one from specialized literature [11]. Large pressure gradient is noted between the shroud-side and hub-side upstream

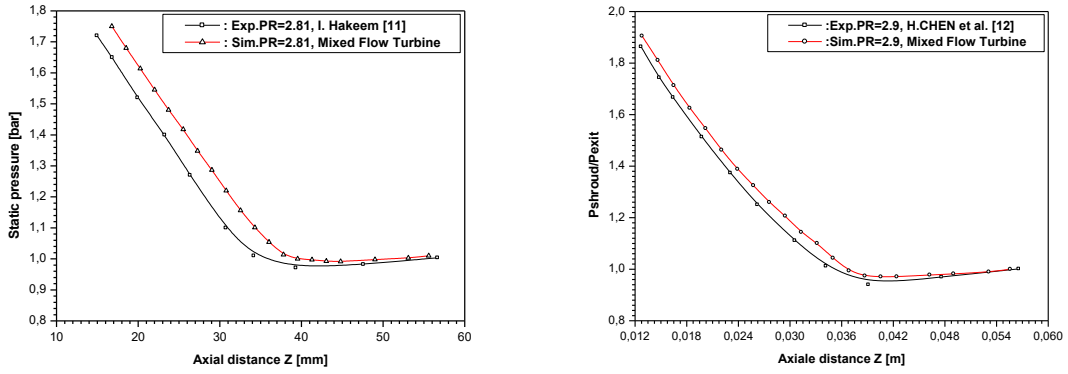

Figure 8: Validation of static pressure distribution along the shroud of MFT

pressure at the rotor inlet with remarkable higher pressure at the shroud-side. This pressure gradient is necessary to stabilize or balance the difference in the centrifugal force between the shroud and hub which arise due to the change in radius from hub to shroud.

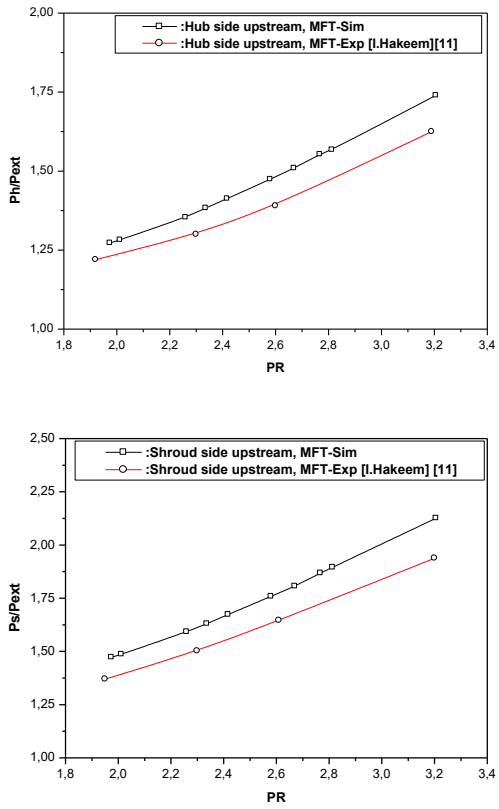

Figure 9: Validation of wall static pressure distribution along the shroud and hub sides of MFT

Furthermore, and as mentioned [11], this pressure gradient will result in high swallowing capacity of the mixed-flow turbine. Finally, another point to be mentioned from Figure 9 is that the shroud pressure is almost a linear function for the range of pressure ratios, which is not the case within the hub pressure. The latter is a parabolic function of the pressure ratios.

5.2 Results from the transient state solution

The flow in the exhaust manifold of an internal combustion engine is highly unsteady due to the opening and closing of the valves. Consequently, flow in a turbocharger turbine is also highly unsteady in nature as it responds to the pressure pulses intrinsic to the exhaust manifold. To reproduce the hysteresis effects existed under pulsating flow conditions, unsteady effects should be considered in any turbine significant numerical study.

5.2.1 Performances of mixed-flow turbine

Figure 10 shows the main performances of MFT turbine under transient operating conditions. Torque and power are compared versus engine speed and to the measured engine torque and power provided by the engine manufacturer from experimental tests. The objective of the comparison between the turbine performances (torque and power) with that of the corresponding engines is to distinguish the correlation nature between the two entities. As depicted in Figure 10 (a), it is noticed that for low engine speed, turbine torque is of higher values and then, it begins to decline within the engine speed increase according to nearly parabolic curve. Torque of MFT rotor is unlikely to exceed (2%) of the engine torque but their use in the engine turbocharging system can increase overall thermal efficiency by

about (3 to 5) %. The most important condition for the turbine is that it will be capable of giving the necessary torque to drive the compressor during delivery at its maximum pressure ratio [1].

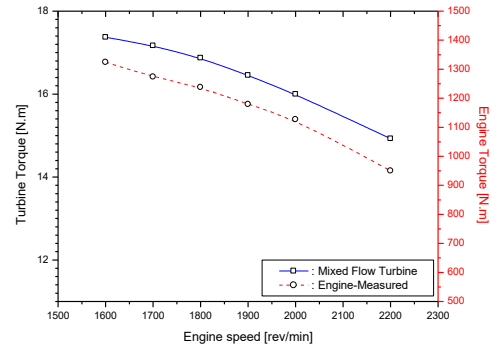

(a)

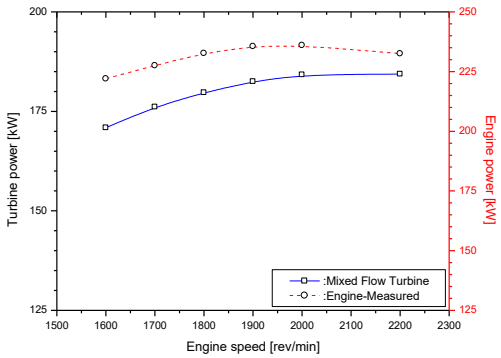

(b)

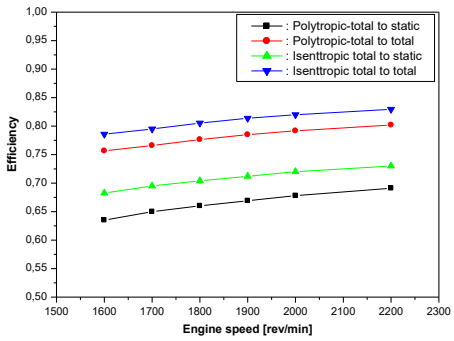

(c)

Figure 10: Mixed flow turbine performances

For the power and as shown in Figure 10 (b), it is noticed that for low engine speed, turbine power is of lower values and then, it begins to slightly rise within the engine speed increase according to nearly linear curve. Power of MFT rotor and because of the higher turbine velocities, it can reach the (80%) of the engine power. As reported previously in the specialized literature, mixed-flow rotors permit non-zero inlet blade angles to be introduced without departing from the radial blade section criterion [12]. For high loading and powerful use of pulsating peak energy from engines, MFT realize the following features: less flow turning and low incidence losses due to the existence of radial and axial flow entry components, lower moment of inertia that suits the transient response of the turbocharger [13, 14]. In an automotive drive cycle, a turbine which can extract more energy at high pressure ratios and lower rotational speed is almost recommended.

The unsteady polytropic (total-to-static and total-to-total) efficiencies for mixed-flow turbine are shown in Figure 10 (c) plotted against engine speed. Total-to-total polytropic efficiency peak was (0.80) and it occurs at an engine speed of (2200rev/min). However, the total-to-static polytropic efficiency is within a peak value of (0.69) occurring at an engine speed of (2200rev/min). The variation of efficiency with engine speed is found to be uniform and confirms its suitability for use in automotive turbochargers [15].

The unsteady isentropic (total-to-static and total-to-total) efficiencies for mixed-flow turbine are shown in Figure 10 (c) plotted against engine speed. Total-to-total peak efficiency is (0.82) and it is occurring at an engine speed of (2200 rev/min). It is not the case for the total-to-static isentropic efficiency where it is clear from the figure that it is almost higher for the MFT turbine within a peak value of (0.73) occurring at engine speed of (2200rev/min).

5.2.2 Blade loading of mixed-flow turbine

Comparison of blade loading diagrams for mixed-flow turbine is presented in Figure 11, at hub, mid-span and shroud sections against engine speed. From the diagrams, the following remarks can be noted: First, as observed, the blade loading variations are affected by three parameters, streamwise direction, spanwise direction and the engine speed (the pulse frequency). According to the spanwise direction, we observe a lower blade loading at hub except in the area near the leading edge, where the blade loading is of higher values. Then, it increases gradually from blades inlet to become with moderate values towards the middle of the stream direction at mid-span. At shroud sections, generally, the blade loading is of higher

values along the whole blade. According to the streamwise direction, the decrease of blade loading along the streamwise direction, is observed in particular at hub, and higher values at the medium of this direction for shroud section. According to the engine speed, for low regimes, the blade loading will reach higher values at the blades leading edge (BLE). For the high regimes, the blade loading is weak compared to the previous.

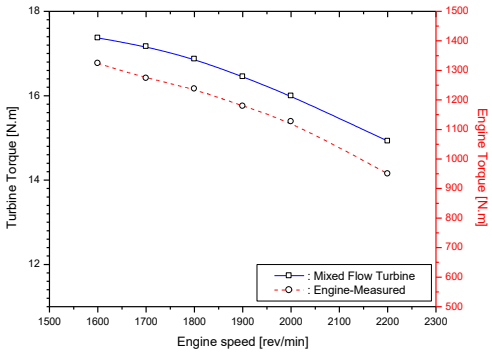

(a)

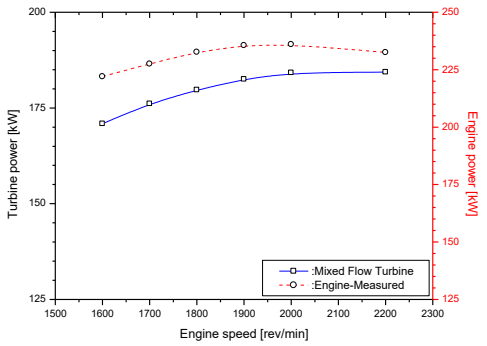

(b)

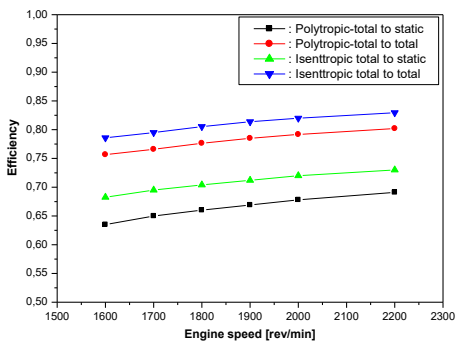

(c)

Figure 11: Blade loading for mixed-flow turbine at pulse peak

Turbochargers are always designed to operate at maximal torque regimes and eventually, at lower speed and full torque. Generally, the blade loading curve shape is almost regular from an engine regime to another. Finally, it is worth mentioning that blade loading check accomplish an important role for the sizing and design of the turbine rotor (blade number and weight) and to prevent various types of turbine losses.

5.2.3 Cyclic pulsating pressure through mixed-flow turbine

Figure 12 shows the pulsating pressure during the exhaust gas cycle through the turbine volute entries for four engine regimes (1600, 1800, 2000 and 2200) rev/min. It is noted that there are always two pressure peaks for each entry; a high peak and a lower one due to the simultaneous opening of two exhaust valves but with time lag of 120°.

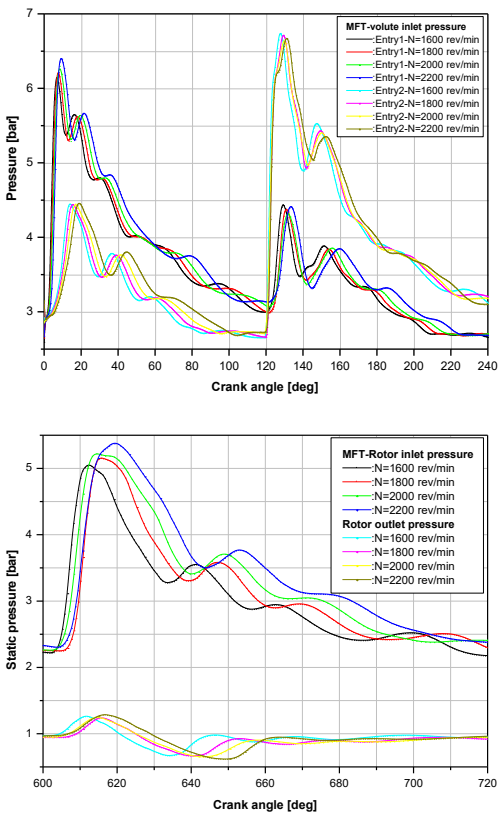

Figure 12: Volute inlet, rotor inlet and rotor outlet pressure for mixed flow turbine

At entry-1 (through the inner limb, Figure 13) and at the exhaust valve opening (from cylinder-2, according to the exhaust phases succession), a high peak is observed during the blow down of the exhaust phase, which is followed by a hyperbolic decrease during the piston displacement of the

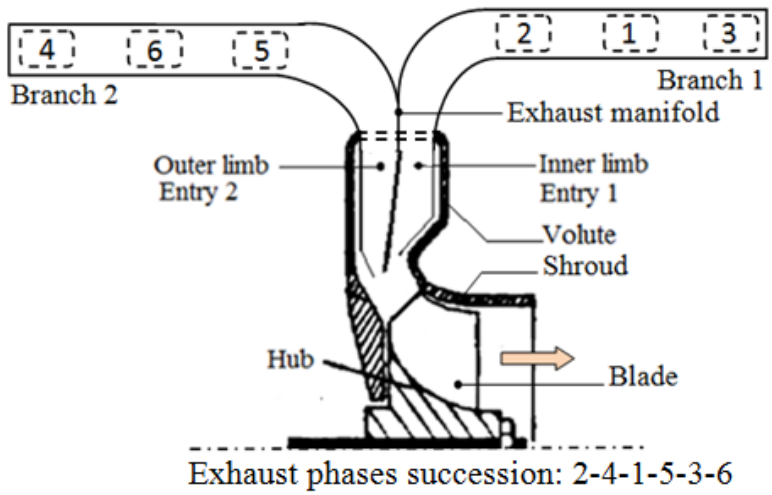

Figure 13: Geometric description of the model

exhaust phase until the opening of the next exhaust valve. At the same time, at entry-2 (through the outer limb, Figure 13), and due to the continuous flow coming from another cylinder in branch-2, a lower peak of pressure is noticed, which is followed by the same evolution as that of the high peak (from cylinder-4, according to the exhaust phases succession).

At the opening of the next exhaust valve, the same sequence of events is repeated at the two entries but with reverse pressure peaks (lower peak at entry-1 and high peak at entry-2). With engine regimes, it is observed that for the first half of the exhaust gas cycle through the volute, the boost pressure is accompanied with the increase in engine speed. For the second half and due to the influences of the previous events at entry-1 (the reinforcement of pressure waves), peak maxima of the pressure increase compared to that of the first half period of exhaust gas cycle through the turbine volute. In the same Figure 12 and for the exhaust gas through the turbine rotor, pressure peaks increase via increasing the engine speed at the rotor inlet. At the rotor outlet, pressure values tend to boost towards the atmospheric pressure, which is confirmed by the gas dynamics consideration.

5.2.4 Cyclic mass flow rate through mixed-flow turbine

Figure 14 shows mass flow rate evolution through the turbine volute and that across the inlet-outlet turbine rotor. As pressure changes, at the opening of the exhaust valve, a high mass flow rate peak is observed at entry-1 (through the inner limb) of the volute. The latter peak corresponds to the blow down of the exhaust phase, which is

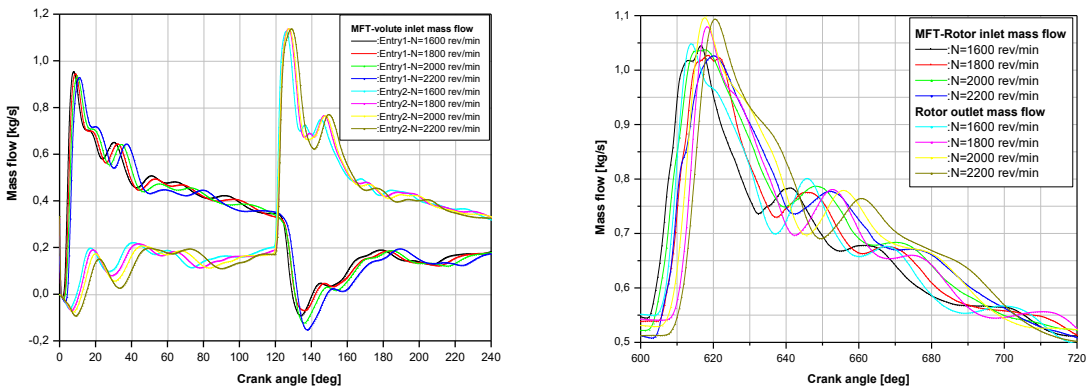

Figure 14: Volute inlet, rotor inlet and rotor outlet mass flow rate for mixed flow turbine

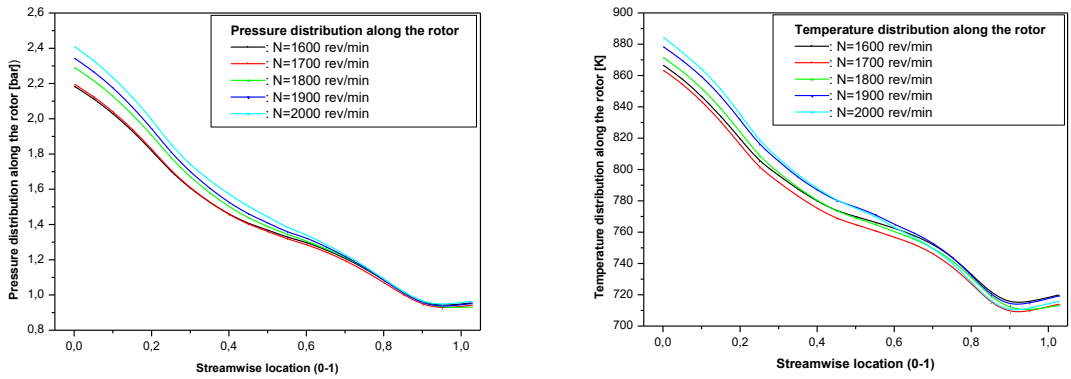

Figure 15: Pressure and temperature distributions along the rotor of MFT

followed by a slow decrease until the opening of the next exhaust valve. In the same time, at entry-2 (through the outer limb), a negative mass flow rate is observed during a small time due to reverse flow from entry-1 to the exhaust manifold. After that, and with emptying process of the turbine volute, a slight increase of mass flow rate at entry-2 is observed until the opening of the next exhaust valve.

At the opening of the next exhaust valve, relative to the engine cylinder which leads to the volute entry-2, the same sequence of events is repeated with reverse manner of mass flow rate peaks. With engine regimes, it is observed that mass flow rate increases by increasing the engine speed. From the same Figure 14, across this rotor type, mass flow rate difference is quite remarkable. Mass flow rate peaks for the different engine regimes at the rotor outlet are greater than that at the rotor inlet, which reflect the favorable emptying process (swallowing capacity).

5.2.5 Pressure and temperature distributions along the rotor of MFT

Figure 15 shows pressure and temperature evolutions from the inlet to the outlet of MFT rotor. Generally, and for the two parameters p and T, a Gaussian or exponential decay is observed. From the inlet, pressures and temperatures increase by increasing the engine regimes. However, pressure curves and temperature distributions, each other converge towards the unique one at the last quarter of the streamwise distance for the MFT. For the temperature, the average value calculated at the outlet (710 K) approaches the measured one (640 K, given by the designer), 10% of difference between the two values.

5.2.6 Flow structure

Flow structure leads to obtain a 3D flow description and which in turn helps to make an initial estimation on the flow regularity. Meridian static pressure contours at the two cases (maximal pulse pressure and the minimal pulse pressure) for engine regime of (2000 rev/min, f=100 Hz) are represented on (Figure 16). It is noticed that the overall static pressure rise with the increase of the engine regime. It is noted that for a given pressure pulse, MFT rotor, always operate at the required values of static pressure (greater than 2 bar). So, the functioning of the turbine is ensured even at the extreme conditions until the beginning of the next pressure pulse. Again, it is observed in the two cases of low mass flow or high mass flow through the turbine that, meridional static pressure from outer limb is always greater than that from the inner limb. Finally, at the maximal pulse pressure, the maximum values of static pressure for the flow crossing the volute limbs are just due to the flow source location from the exhaust manifold (Figure 13). Whenever the source is distant, it leads to the reinforcement of pressure waves and hence, to boost pressure.

Meridional tangential relative velocity vectors in both cases i.e., the impact of the turbine blades and the maximal pulse pressure, for the engine regimes of (1600 and 2000) rev/min are illustrated on (Figure 17 and Figure 18). At the impact of turbine blades and for the flow coming from the inner limb, the emergency of two recirculation zones is observed as the engine regimes increase gradually. The first, the smallest, just after the balde-in, near shroud wall and the second, which is the biggest, just before the blade-out near rotor hub. For the flow coming

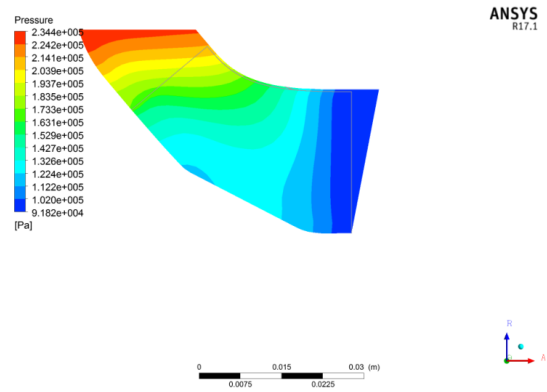

At minimal pulse pressure
(low mass flow-inner limb)

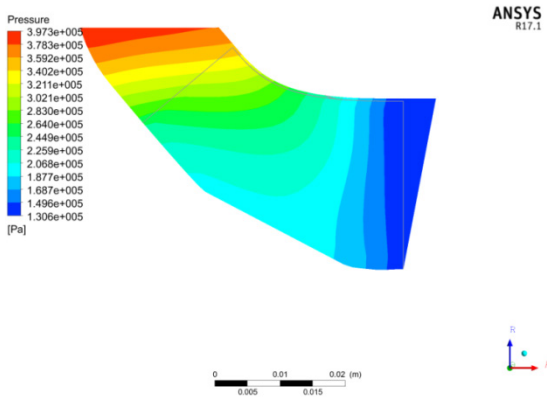

At maximal pulse pressure
(high mass flow-inner limb)

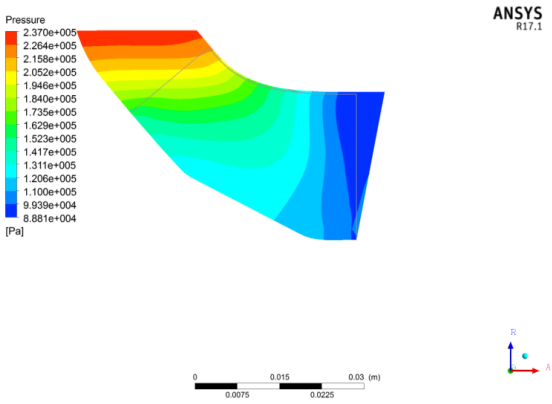

At minimal pulse pressure
(low mass flow- outer limb)

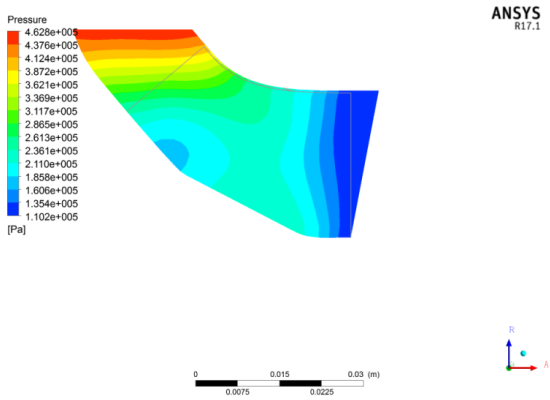

At maximal pulse pressure
(high mass flow- outer limb)

Fig. 16: Meridian static pressure contours (N=2000 rev/min-f=100 Hz)

from the outer limb, in the case of low regimes, flow acceleration at the blade-in near hub is observed, followed by a recirculation zone. The latter, leads to accelerated flow deflection towards shroud wall. With engine regimes rise, recirculation zones disappears but the accelerated flow at the blade-in near hub still persists.

In the case of maximal pulse pressure (Figure 18) and for the flow coming from the inner limb, tangential velocity vectors are almost uniform from hub to shroud and are gradually accelerated from inlet to outlet. For the flow across the outer limb, localization of recirculation zone near-hub is still present, which leads to the deflection of accelerated flow from hub to shroud.

6. Conclusion

Actually, matching of the turbocharger to the engine can be carried out meticulously by thermodynamic and gas dynamic analysis. The flow in the exhaust manifold of an internal combustion engine is highly unsteady due to the opening and closing of the valves. Consequently, flow in a turbocharger turbine is also highly unsteady in nature as it responds to the pressure pulses intrinsic to the exhaust manifold. To reproduce the hysteresis effects existed under pulsating flow conditions, unsteady effects should be considered in any turbine significant numerical study. Using theory and numerical techniques, a thermodynamic model was developed and implemented for the gas

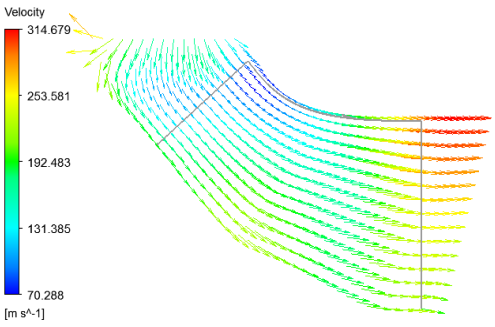

N=1600 rev/min-f=80 Hz-inner limb

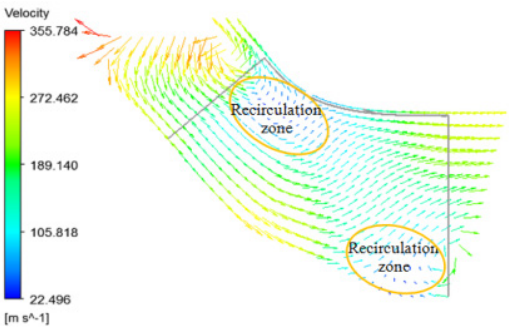

N=2000 rev/min-f=100 Hz-inner limb

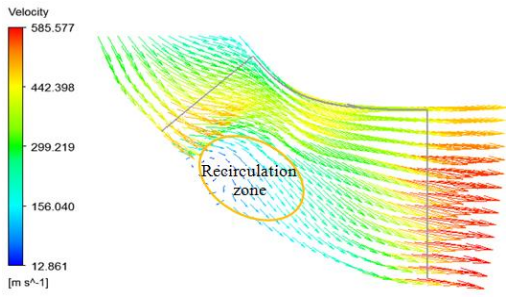

N=1600 rev/min-f=80 Hz-outer limb

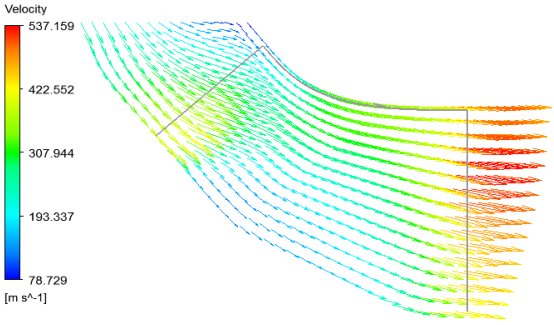

N=2000 rev/min-f=100 Hz-outer limb

Fig. 17: Tangential relative velocity vectors on meridian view at the impact of the turbine blades

expansion process through the exhaust system of turbocharged internal combustion engines. The model was used to setup the unsteady state analysis using 3D simulation, it was an attempt to investigate pulsating flows under transient conditions.

In this study, the thermodynamic model proposed is used to characterize the flow behavior and to evaluate the main performances of mixed flow turbine. The latter is the geometrically complex and operational component of exhaust gas circuit, it is the power source of the compressor rotor.

From the tested case, the remarkable findings can be drawn: regular gas expansion and better conversion process of energy recovered from engine exhaust gases to drive this type of rotor (MFT). Large pressure gradient is noted between the shroud-side and hub-side upstream pressure at the rotor inlet. This pressure gradient will result in high swallowing capacity of the mixed-flow turbine. Mixed-flow turbine torque and power are almost higher. Torque is unlikely to exceed (2%) of the engine torque but their use in the engine turbocharging system can increase the overall thermal efficiency by about (3 to 5)%. Power can reach (80%) of the engine power because of the higher turbine velocities.

Check of blade loading accomplishes an important role for the sizing and design of the turbine rotor (blade number and weight) and prevents the various types of turbine losses. In this study, it is observed that the blade loading variations are affected by three parameters, streamwise direction, spanwise direction and the engine speed. According to the engine speed, it is observed that for low regimes, the blade loading will reach higher values at the blades leading edge (BLE).

Mass flow rate peaks for the different engine regimes at the rotor outlet are greater than that at the rotor inlet, which reflect the favorable emptying process or swallowing capacity of MFT. Also, it is observed that mass flow rate at the turbine volute entries, decreases by increasing the engine speed.

For cyclic pulsating pressure, it is always noted that there are two pressure peaks at the volute inlets, a high peak and a lower one due to the simultaneous opening of two exhaust valves with time lag of 120° for the six cylinder-four strokes

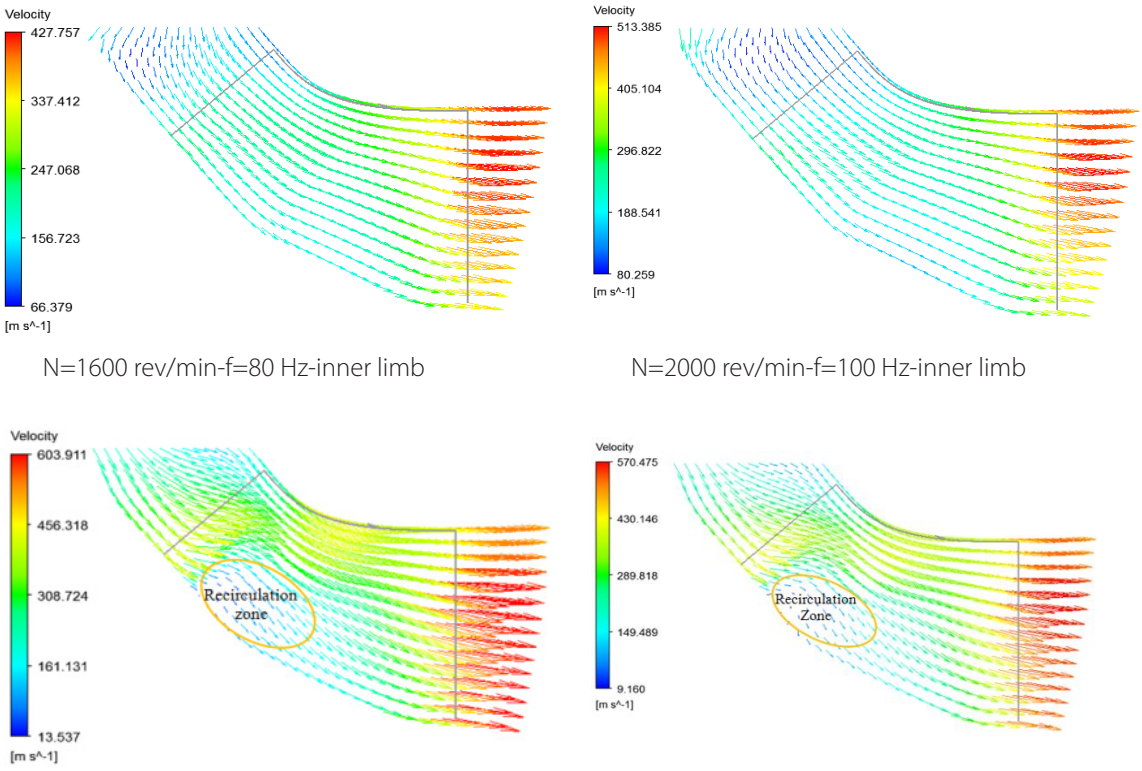

Fig. 18: Tangential relative velocity vectors on meridian view at maximal pulse pressure

ICE. For the exhaust gas through the turbine rotors, it is observed that pressure peaks increases by increasing the engine speeds at the rotor inlet. At the rotor outlet, pressure values tend towards the atmospheric pressure, which is confirmed by the gas dynamics consideration. Pressure evolution from the inlet to the outlet of the two types of turbine rotors exhibit a Gaussian decay.

From meridian pressure contours it is noted that for a given pressure pulse, MFT rotor always operate at the required values of static pressure. So, turbine functioning is ensured even at the extreme conditions until the beginning of the next pressure pulse. At maximal pulse pressure, the maximum values of static pressure for the flow crossing the volute limbs are just due to the flow source location from the exhaust manifold. Whenever the source is distant, it leads to the reinforcement of pressure waves and hence, to boost pressure.

References

[1.] Garrett T. K., Newton K. and Steeds W (2001). The Motor Vehicle, 13th ed, Butterworth-Heinemann, Oxford.

[2.] Stobart R. and Weerasinghe R. (2006). Heat Recovery and Bottoming Cycles for SI and CI Engines-A Perspective. SAE Paper 2006-01-0662.

[3.] Liu J. P., Fu J. Q., Reu C. Q., Wang L. J., Xu Z. X. and Deng B. L. (2013). Comparison and analysis of engine exhaust gas energy recovery potential through various bottom cycles. Applied Thermal Engineering, 50(1), 1219-1234.

[4.] Haddad S. D. and Watson N (1984). Principles and Performance in Diesel Engineering, Ellis Horwood Ltd.

[5.] Challen B. and Baranescu R (1999). Diesel Engine Reference Book, 2nd ed, Butterworth-Heinemann, Oxford.

[6.] Ramos J. I (1989). Internal combustion engine modelling, Hemisphere Publishing Corporation.

[7.] Winterbone D. E. and Pearson R. J (2000). Theory of Engine Manifold Design. Wave Action Method for IC Engines,

Professional Engineering Publishing Limited London and Bury st Edmunds.

[8.] Menter F. R. (1994). Two-Equation Eddy-Viscosity Turbulence Models for Engineering Applications, AIAA Journal. 32 (8):1598-1605.

[9.] Rakopoulos C. D. and Giakoumis E. G. (2004). Availability analysis of turbocharged diesel engine operating under transient load conditions. Energy, 29 (8):1085-1104.

[10.] Launder B. E. and Spalding D. B. (1974). The numerical computation of turbulent flows. Computer Methods in Applied Mechanics and Engineering, 3(2): 269-289.

[11.] Hakeem I. (1998). The effects of rotor geometry on the performance of mixed-flow turbocharger turbines. J. eng.& appl. Sci, 17(1): 145-164.

[12.] Chen H., Abidat M., Baines N. C. and Firth M. R. (1992). The effects of blade loading in radial and mixed flow turbines. Paper No: 92-GT-092, V001T01A049-ASME.

[13.] Baines N. (2002). Radial and Mixed Flow Turbine Options For High Boost Turbochargers. 7th International Conference On Turbochargers and Turbocharging, London, May 14-15.

[14.] Ramesh K., Prasad BVSS. and Sridhara K. (2019). A comparative study of the performance of the mixed flow and radial flow variable geometry turbines for automotive turbocharger. Proc.IMechE PartC, J Mechanical Engineering Science, vol. 233(8) 2696-2712.

[15.] Arcoumanis C., Hakeem I., Khezzar L., Martinez-Botas R. F. and Baines N. C. (1995). Performance of mixed flow turbocharger turbine under pulsating flow conditions. Paper No: 95-GT-210, V002T04A011-ASME.